In situ deposition/positioning of magnetic nanoparticles with ferroelectric nanolithography

Xiaojun Lei, Dongbo Li, Rui Shao, and Dawn A. Bonnell[a)]
Department of Materials Science and Engineering, The University of Pennsylvania, Philadelphia, Pennsylvania 19104

(Received 17 August 2004; accepted 13 December 2004)

Ferroelectric nanolithography is a new approach to processing nanostructures, which can position multiple components made of various materials into predefined configurations. Local polarization in ferroelectric compounds is manipulated to control the surface electronic structure and direct attachment of molecules and particles. Here, the presence of optically excited electron-hole pairs on ferroelectric domains is confirmed, and reaction paths for photo reduction of several reactive metal particles are determined. Subsequent and simultaneous deposition of multiple metals is demonstrated, and the magnetic properties of Co based particles are confirmed.

I. INTRODUCTION

Over the last five years there has been an explosion in the synthesis of new functional nanostructures, i.e., tubes, wires, dots, synthetic biological molecules, etc.[1] To exploit these structures in devices, concomitant advances in materials processing are required. Interesting approaches have been developed for some specific applications. The first nanolithographies were based on scanning probes, which are not considered practical, except in specific niche applications.[2] Microcontact printing has become a common method of patterning self-assembled monolayers.[3] Nanoimprint lithography and "step and flash" lithography have been developed to pattern semiconductor photo resists.[4,5] DNA and protein directed assembly have been used to control nanoparticle assembly.[6–8] Dip-pen lithography and similar approaches based on ink jet printer strategies are finding use in specific applications such as array chips.[9,10] Finally electric, magnetic or mechanical fields have been used to align nanostructures, for example as is practiced in electrophoretic assembly.[11,12] These strategies are successful in producing patterns or arrays of particles, molecules, wires, or tubes, generally operating on one class of material at a time.

Recently Kalinin et al.[13] proposed a directed assembly process, ferroelectric nanolithography, which can position multiple components made of various materials into predefined configurations. The approach is based on observations of orientation- and domain-dependent chemical reactivity.[14–16] Ferroelectric nanolithography utilizes atomic polarization in ferroelectric compounds to control the surface electronic structure and direct attachment of molecules and particles. The earlier work demonstrated the process on photo reduction of inert metals to produce nanometer-sized particles and attachment of functionalized organic molecules. The process has the potential to be completely general, operating on reactive metals, functionalized nanowires, tubes, and dots as well as biological molecules, but these processes have not yet been demonstrated and are not understood at a fundamental level.

This paper reports the controlled patterning of cobalt-, nickel-, and iron-based nanoparticles, subsequent and simultaneous deposition of multiple metals, and the magnetic properties of some particles.

II. EXPERIMENTAL PROCEDURES

Lead zirconate titanate (PZT) thin films were prepared by a sol-gel method on a $Pt/SiO_2/Si$ substrate with a Zr/Ti ratio of 53/47. The film thickness was ~200 nm, and characteristic grain size was 50–100 nm. [In sol-gel processing, a lead acetate and zirconium propoxide are dissolved in alcohol to form a precursor sol. Films are deposited by dip coating onto an oxidized silicon wafer coated with a Pt film followed by annealing.] The typical microstructure of the films, illustrated in Fig. 1, exhibits homogeneous distribution of grains with maximum root-mean-square roughness of 5.7 nm over 5×5 micro square.

Local polarization orientation on the substrates was patterned with scanning-probe microscopy and with e-beam lithography[17] and piezoresponse force microscopy (PFM) was used to confirm the domain orientation. Contact-mode atomic force microscopy (AFM) was performed on a commercial instrument (Digital Instruments Dimension 3000 NS-III, Veeco Instruments, Inc.,

a)Address all correspondence to this author.
e-mail: Bonnell@lrsm.upenn.edu
DOI: 10.1557/JMR.2005.0093

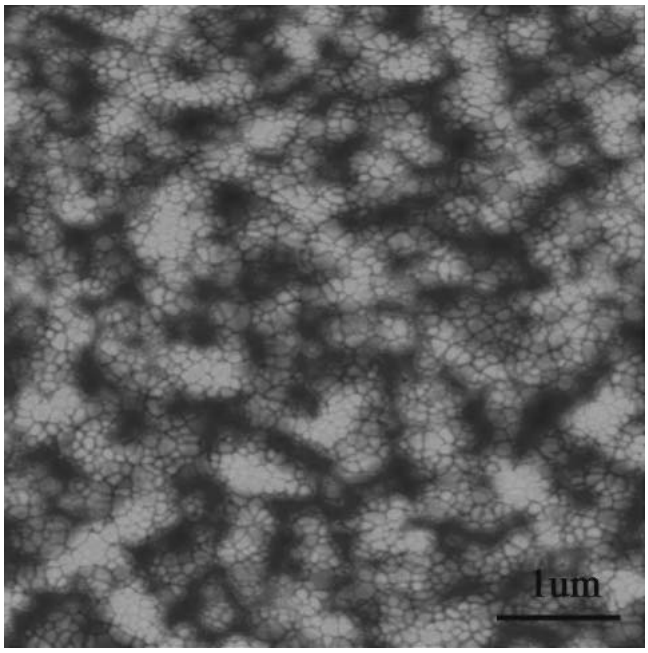

FIG. 1. Topographic structure of PZT thin films. Vertical scale (dark to light) is 50 nm.

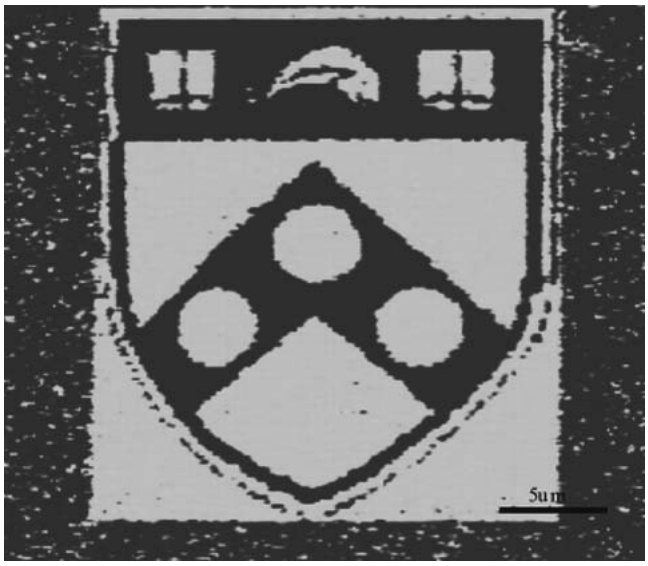

FIG. 2. PFM image of a complex domain pattern on a PZT thin film. The contrast in the image corresponds to the orientation of polarization; light contrast indicates c+ domains and dark contrast indicates c− domains. The random orientation of ~100 nm grains outside of the pattern is also observed.

Woodbury, NY). For PFM the AFM was equipped with a function generator and lock-in amplifier (DS340, SRS 830, Stanford Research Systems, Sunnyvale, CA) and high voltage power supply (PS310, Stanford Research Systems). To protect the electronic system, the electrical connections between the microscope and the tip were severed. Gold-coated tips (L ≈ 125 μm, resonant frequency ~350 kHz, Micromasch NSCS12 W2C, Mikromasch, Portland, OR) were used for these measurements. The domains in the PZT substrates were patterned by applying ±10 V between an AFM tip and the sample. Figure 2 illustrates an example of complex patterns of oriented domains that can be achieved on thin film substrates, demonstrating the potential to make devices requiring sophisticated patterns.

After patterning, samples were submerged in the aqueous metal salt solutions made from $AgNO_3$, $HAuCl_4$, $H_2PtCl_6.6H_2O$, $RhCl_3$, $PdCl_2$, $NiCl_2.H_2O$, $FeCl_3$, $FeCl_2$, and $CoCl_2{\cdot}6H_2O$ at room temperature. Concentrations ranged from 10^{-2} M to 10^{-6} M and reaction time from 5 to 120 min. A Hg/Xe arc lamp with a 500 W power supply (66011, 68811, Oriel Instruments, Stratford, CT) was used to irradiate the samples. Metal nanoparticles on PZT thin films were characterized by optical microscopy, electron microscopy (JEOL 6300FV SEM, JEOL USA, Inc., Peabody, MA) or AFM after exposure. To facilitate rapid analysis of reaction products for this study, the pattern feature sizes were on the order of 500 nm to 100 μm; however, spatial resolution as a high as 10 nm can be achieved.

The reaction mechanism is based on electron exchange at the surface. Figure 3 illustrates the energies associated

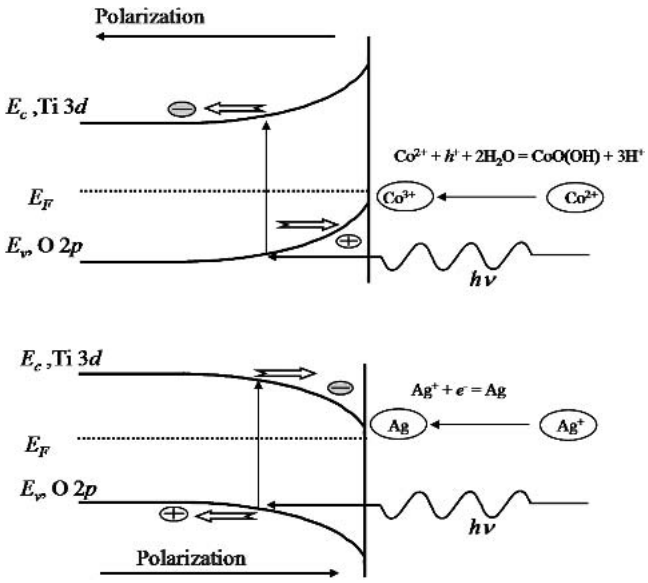

FIG. 3. Schematic diagram of photo reactions. Electron-holes generated by optical absorption in a wide band gap compound migrate in the local field near the surface. The band bending is a consequence of surface charge that results from polarization and is domain specific. Oxidation reactions occur at c− domains while reduction occurs at c+ domains.

with the process. If described in semiconductor terminology, the valence band edge in PZT consists primarily of the oxygen 2*p* orbital, while the conduction band edge is derived from the Ti 3*d* orbital. The dipole interactions responsible for the formation of domains result in a charge at the termination of a crystal, i.e., at the surface. This charge will locally alter the energies of the bands as

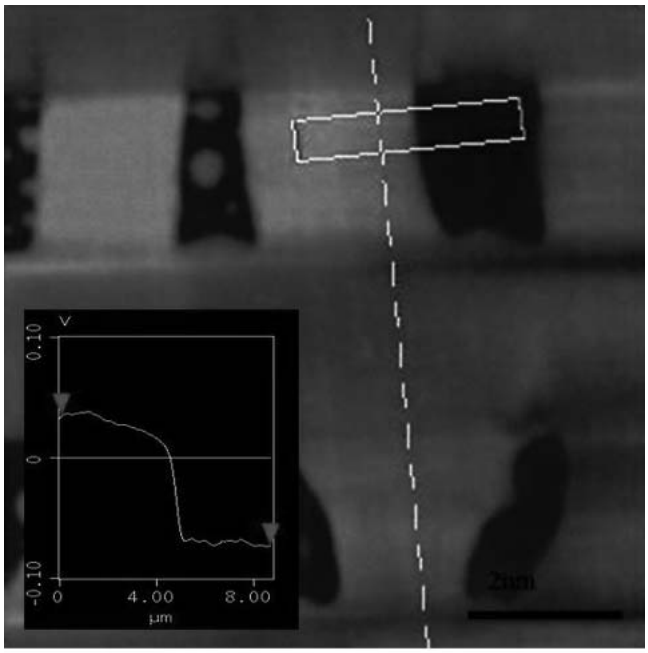

(a)

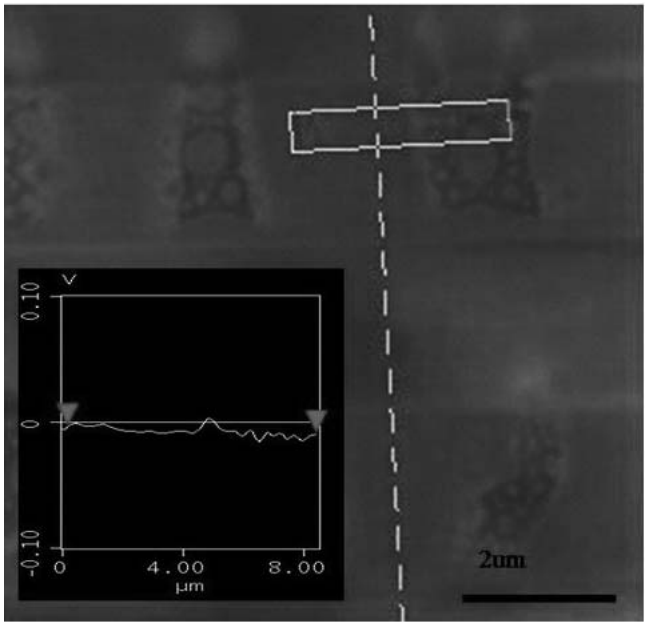

(b)

FIG. 4. Scanning surface potential images of $BaTiO_3$ showing the difference in potential between c+ and c− domains (a) before and (b) during illumination with a UV source. The line scans in the insets quantify the difference as 120 MeV before irradiation and 10 MeV during radiation.

illustrated in Fig. 3. In those areas experiencing upward band bending, electrons cannot be donated by the substrate to form a nanostructure, while in those experiencing downward band bending electron transfer can occur. However, upward band bending does allow electron exchange to the sample. Since the mobile carrier concentration in PZT is extremely low, optical excitation is required to produce electron-hole pairs. The effect of the electron-hole pair generation on surface potential is illustrated in Fig. 4 for a $BaTiO_3$ (100) single crystal. The difference in potential between upward (c+) and downward (c−) oriented domains observed under ambient conditions is a complex combination of polarization and screening and is on the order of 120–150 MeV.[18–20] Upon irradiation, the difference reduces to 10 MeV due to a combination of desorption and diffusion of carriers to the surface. This interaction is somewhat complicated and discussed in detail in Ref. 21. Nevertheless, the time dependence of the potential difference demonstrates that the diffusion of electrons and holes in response to electric-field gradients near the surface plays a large role in polarization compensation. These carriers are available to participate in chemical reactions.

III. RESULTS AND DISCUSSION

Figure 5 indicates how the wavelength dependence of the electron exchange is related to the band gap of the

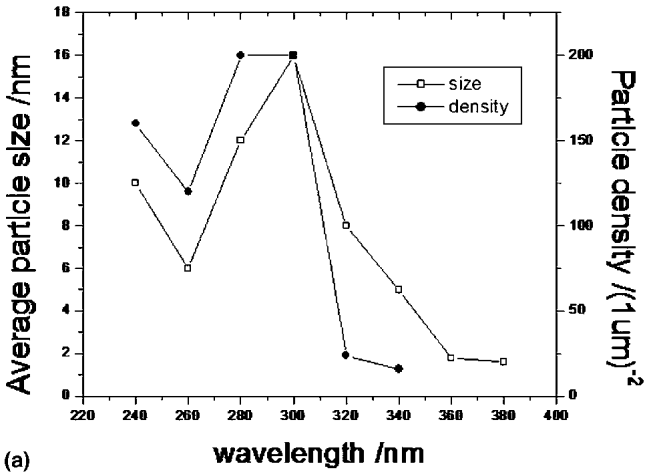

(a)

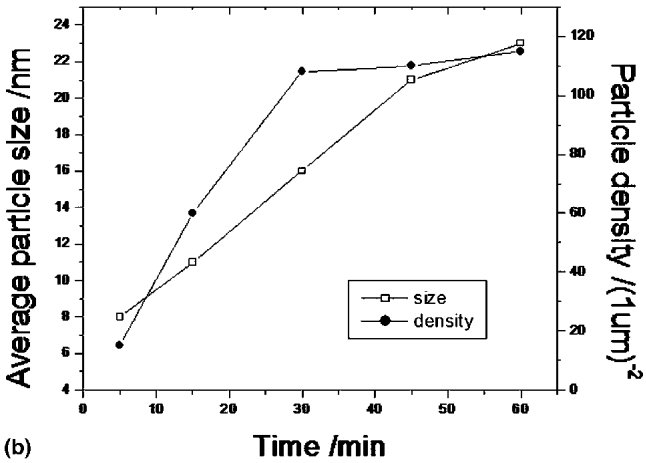

(b)

FIG. 5. Wavelength and time dependence of particle size and density for Ag photo reduced from 10^{-4} M solution, 300 W power UV light. The wavelength dependence of reaction for (a) 30 min is compared to the time dependence at (b) 300 nm.

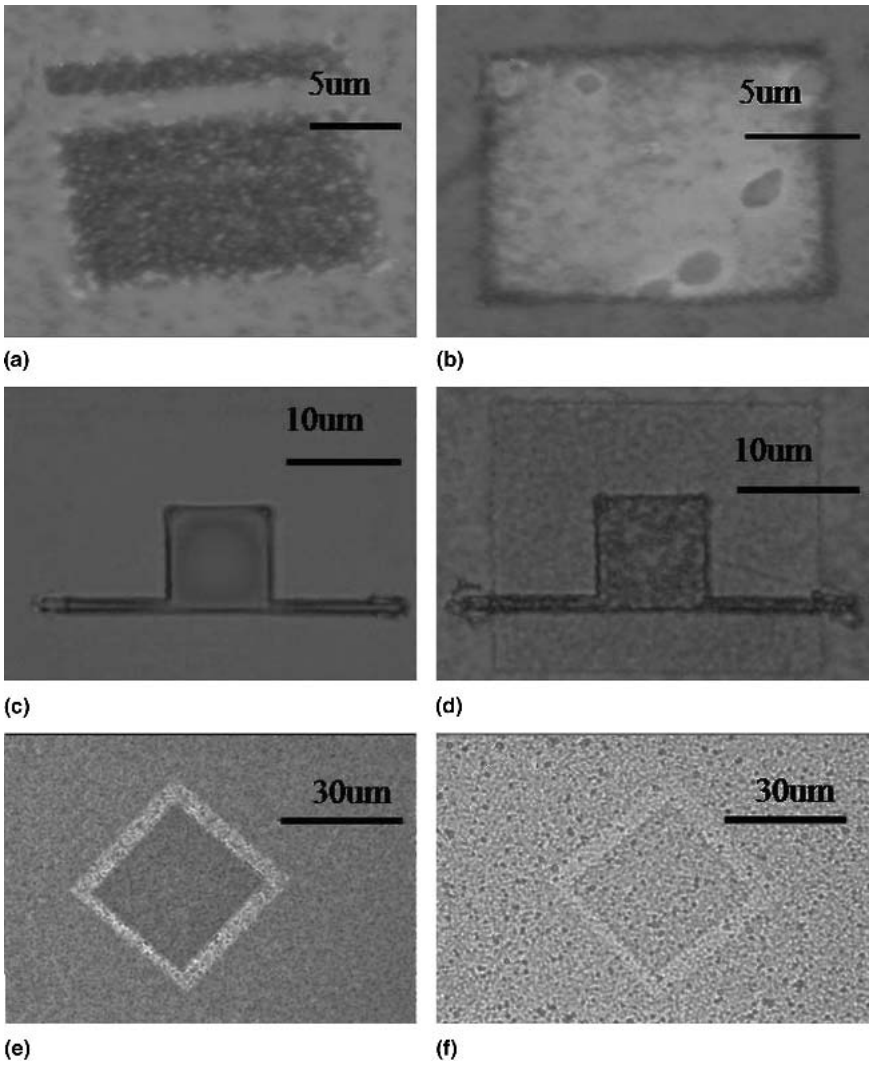

FIG. 6. Optical micrographs of nanoparticles photoreacted on patterned PZT substrates. Three multiply metal processes are illustrated: (a) Ag and Au sequentially deposited on c+ domains, (b) Au and Ag simultaneously deposited on c+ domains, (c) Co-based particles deposited on c− domains, and (d) Co-based particles on c− domains followed by Au on c+ domains, (e) Ni on c+ domains, and (f) Fe on c+. Due to the roughness of PZT substrate and measurement of the experimenter, there is about a 1–2 nm deviation on average particle size points.

substrate by comparing particle size and density for the precipitation of Ag from 10^{-4} M solution at room temperature. Due to the effect of the convolution of the AFM tip on particle diameter, particles size was estimated from the height assuming the particles adopt a nearly spherical shape. Uncertainty in the particle size and density is significant when the particle size approaches the dimension of the substrate roughness; nevertheless, several important observations can be made. The wavelength dependence can be divided into three regions. Between 360 and 380 nm, no clear patterns were formed and the observed feature sizes were close to that of original PZT substrate. Between 320 and 340 nm, larger identifiable particles (8 and 5 nm) and density ($24/(\mu m)^2$ and $16/(\mu m)^2$) were obtained with the maxima occurring between 240 and 300 nm. Therefore, the reaction threshold is 4.1 eV (corresponding to 300 nm), which is 0.5 eV above the substrate band gap, 3.6 eV. The energy in excess of the bandgap enables the exchange from the surface to the ion.

TABLE I. Summary of successful photoreactions.

Reagents	Products	Reduce potential
$AgNO_3$	Ag	0.799 (acidic)
$HAuCl_4$	Au	1.002 (acidic)
$H_2PtCl_6 \cdot 6H_2O$	Pt	1.188 (acidic)
$RhCl_3$	Rh	0.76 (acidic)
$PdCl_2$	Pd	0.915 (acidic)
$NiCl_2 \cdot xH_2O$	Ni	−0.72/−0.257 (basic/acidic)
$CoCl_2 \cdot xH_2O$	CoO(OH)	−0.42 (basic)
$FeCl_2$	Fe	−0.89/−0.44 (basic/acidic)

As we compare the reduction potentials of the reactions that have been successful (Table I), there is no obvious correlation between reaction rates and reduction potentials. This implies that kinetic considerations dominate over thermodynamics to dictate specific react paths. For example, the silver ion exists as $Ag^{+}(H_2O)_4$ in water while gold has the form of $[AuCl_4]^{-}$. Both have four ligands, but the former noncovalent bonding is easier for an electron to attack than the latter covalent bonding. This is consistent with the observation that under the same conditions the silver reduction rate is much faster than that of gold.

Light intensity at different wavelengths was varied, and no correlation with particle number or density was found. This may result because in the range of intensities used, the reaction is limited by electron transfer to the ions and by diffusion of ions in the liquid. The time dependence of particle size and density exhibits monotonic increases of size by a factor of 3 and of density by a factor of 6 over 60 min. The density reached saturation at 30 min, while particle size continued increasing. The concentration dependence was determined over 5 orders of magnitude. Unsurprisingly, higher concentration yielded larger particle size and higher density.

To be effective in producing complex nanostructures, the nano particles must be sufficiently stable to allow subsequent and/or simultaneous reactions of multiple compounds. Previous studies showed that Ag could be deposited and removed, and then Pd could be subsequently deposited on the same domain. In the present study, multi-element photo deposition was carried out with two processes, sequential deposition and mixed deposition. In sequential deposition, the first metal was deposited on the substrate from a salt solution, and then the deposition process was repeated with a second metal solution. Figure 6(a) shows that silver then gold deposition from 10^{-4} M and 10^{-3} M solutions respectively, for 30 min resulted in layers of Au nanoparticles on top of Ag nanoparticles. Under these conditions particles of approximately 80 nm completely covered the positive domains. For simultaneous deposition a solution was prepared with two metal ions, the ratio of which was adjusted to control the composition of deposition. Figure 6(b) shows a region on which Ag and Au nano particles deposited on c+ domains from a solution with a concentration ratio of 1:5 (Ag /Au ions) and reaction time of 20 min The resulting structure was a complete coverage of the domain with approximately 50 nm sized particles with a concentration ratio of 3:1 (Ag/Au). The bi metallic deposition was observed by SEM, and the presence of metals was quantified by EDS. Clearly the deposition rates of the two metals are not equal.

To extend this approach to a broader materials set, reactions for a wide range of metal-based particles were developed. Table I summarizes the reaction conditions that produced particles. In some cases the particles resulted from reduction, in others from oxidation. This can be inferred from whether the reaction occurred at a c+ or c– domain. For example the possible reactions for $FeCl_2$ in this environment are

$$2Fe^{2+} + 2h^{+} + 3H_2O \rightarrow Fe_2O_3 + 6H^{+} \quad , \qquad (1)$$

$$3Fe^{2+} + 2h^{+} + 4H_2O \rightarrow Fe_3O_4 + 8H^{+} \quad , \qquad (2)$$

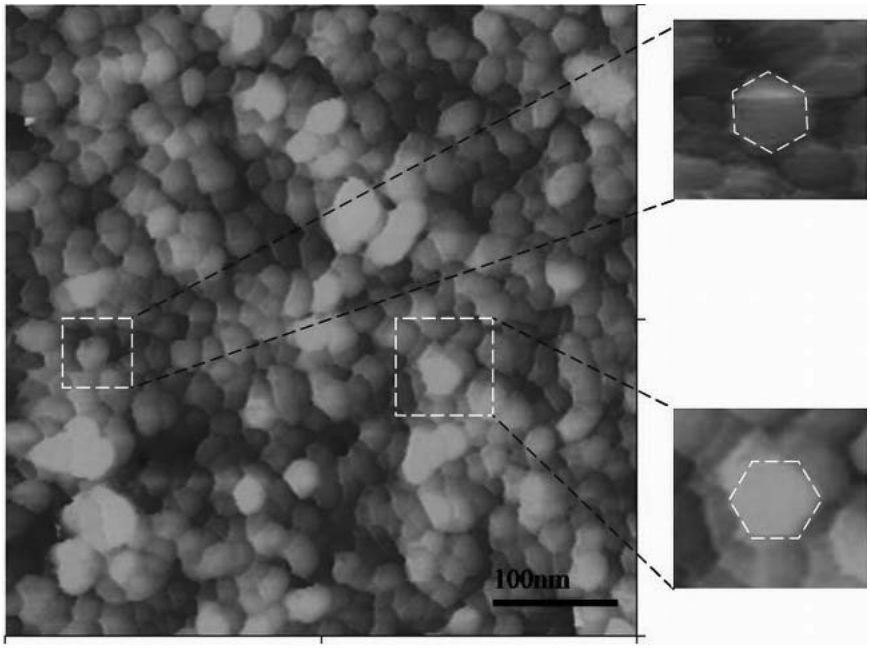

FIG. 7. AFM image of cobalt-based particles. Vertical scale (dark to light) is 50 nm. The insets give morphologies of individual particles.

$$Fe^{2+} + 2e^{-} \rightarrow Fe \quad , \qquad (3)$$

Since the iron based particles deposited over c+ domains, they accepted electrons, i.e., reaction (3). Of course, in an aqueous environment, then the surface of the particle at least is expected to oxidize. The final composition of the particle is not now known. Reaction with a $FeCl_3$ reagent was not successful in producing Fe based particles. A similar argument can be made for the case of Ni. In contrast, Co-based particles were the result of oxidation, occurring over c– domains. Figure 6(c) illustrates cobalt nanoparticles that were produced in a 10^{-3} M $CoCl_2$ aqueous solution with 2 h of exposure of white light [included the ultraviolet (UV) range] on a PZT surface. Topographic analysis in AFM confirmed 250 nm thick deposition over c– domains and the absence of reaction product over c+ domains. In this process Co^{2+} ions lost electrons, existing on the surface with a higher valence, probably its oxide with 3+ valence. The morphology of the cobalt nano particles (Fig. 7) exhibits a tendency toward hexagonal shape. In spite of the rounding effect of tip shape convolution, the particles appear to be faceted and many (most) can be seen to approach hexagonal. This hexagon structure is consistent with the reported structure of single crystal of Cobalt (III) oxide[22] [CoO(OH)] that would be expected on growth near equilibrium conditions.

Since the cobalt and gold nanoparticles undergo opposite electron exchange reactions, it is possible to sequentially deposit these on the appropriate domains. Figure 6(d) is a pattern in which gold nanoparticles surround cobalt oxide nanoparticles, which was made with 15 min of white light exposure in a 10^{-3} M $HAuCl_4$ aqueous solution after 2 h of white light exposure in a 10^{-3} M $CoCl_2$ aqueous solution on a PZT surface. This is similar to the observations by Rorher et al. in which PbO and Ag were deposited on $BaTiO_3$. Nickel and iron based particles were made with 10^{-3} M concentration and 24 min irradiation [Figs. 6(e) and 6(f)].

The magnetic properties of the Co-, Fe-, and Ni-based nanoparticles were examined by magnetic force microscopy (MFM). A cobalt-coated AFM tip was used and verified on a standard magnetic sample before obtaining the MFM image on cobalt nanoparticles shown in Fig. 8. Due to the bluntness of the coated tip, the spatial resolution of topography image was not as high as that obtained with an uncoated tip. Almost every particle in the topographic image appears to have a magnetic signature, although the intensity varies somewhat. That the magnetic force image is not a topographic artifact is confirmed by repeatedly comparing an adjacent non magnetic/magnetic reference sample during the experiment. The fact that the smallest magnetic feature is comparable to the size of a single nanoparticle suggests that each nanoparticle contained only one magnetic domain.

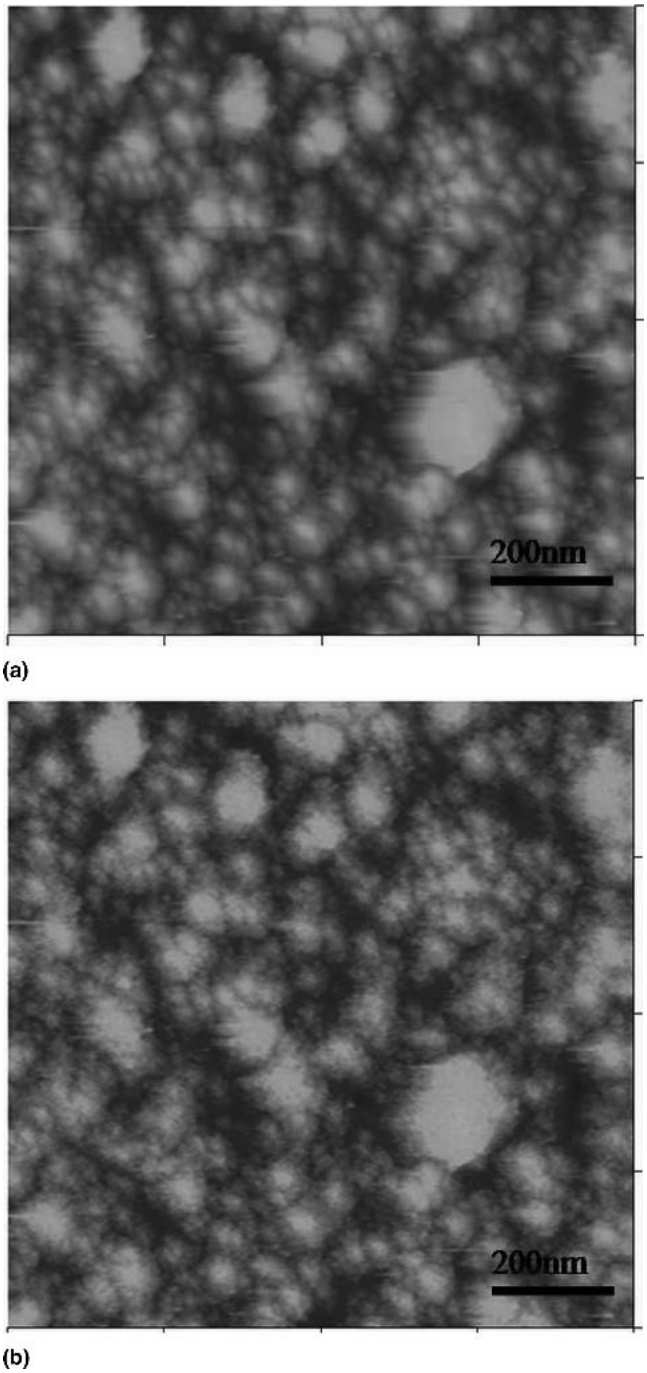

FIG. 8. AFM topographic image (a) and corresponding MFM image (b) on cobalt-based particles. Vertical scales (dark to light) are 50 nm and 10 Hz.

Similarly magnetic nanoparticles of nickel and iron have been analyzed both on PZT thin films and single crystal barium titanate substrates. Magnetic signatures could not be obtained on theses samples, in which the particles were >10 nm diameter. The particles were either nonmagnetic compounds, below the super paramagnetic size limit, or below the signal detection limit of the MFM.

IV. CONCLUSIONS

These results have demonstrated that nanoparticles based on reactive metals can be produced by oxidation and reduction on the surface of ferroelectric substrates upon irradiation with supra band gap light. The optical energy required exceeds that of the band gap by 0.5 eV. Multiple types of nanoparticles can be deposited sequentially and simultaneously. Co-based particles exhibited magnetic properties, while Fe- and Ni-based particles did not, perhaps due to the small size.

Broadening the library of metals that can be patterned expands the ability to tailor contact potential when these particles are used for molecular electronics. Determining reaction paths for reactive transition metal based particles allows ferroelectric nanolithography to be considered for patterning catalysts. The compounds used to catalyze Si based and GaAs based nanowires, carbon nanotubes, and a variety of oxide-based tubes, and wires could now be placed in patterns for directed growth. The broadened base of nanoparticles widens potential to fabricate patterned sensors based on surface enhanced response functions. The demonstration of magnetic particle placement allows information storage applications to be considered. Finally, the robustness of the multiple reaction process enables ferroelectric nanolithography to be applied to more complex structures.

ACKNOWLEDGMENTS

We acknowledge the support from National Science Foundation Grant No. DMR 96-32596 for facilities use, the Center for Science and Engineering of Nanoscale Systems (SENS) at the University of Pennsylvania, and the Department of Education. We have benefited from extensive discussions with John Vohs and S. Dunn.

REFERENCES

1. D.A. Bonnell: Materials in nanotechnology: New structures, new properties, new complexity. *J. Vac. Sci. Technol.* **21,** S194 (2003).
2. H.W.P. Koops, E. Dobisz, and J. Urban: Novel lithography and signal processing with water vapor, in *The Proceedings of Fourth International Conference on Nanometer-Scale Science and Technology,* edited by D.A. Bonnell, T.A. Michalske, X. Shen, and G. Mcguire (1997) p. 1369.
3. Y. Xia and G.M. Whitesides: Soft lithography. *Ann. Rev. Mater. Sci.* **28,** 153 (1998).
4. S.Y. Chou: Nanoimprint lithography and lithographically induced self-assembly. *MRS Bull.* **26,** 512 (2001).
5. B.J. Choi, S.V. Sreenivasan, S. Johnson, M. Colburn, and C.G. Wilson: Design of orientation stages for step and flash imprint lithography. *Precis. Eng.* **25,** 192 (2001).
6. C.J. Loweth, W.B. Caldwell, X. Peng, A.P. Alivisatos, and P.G. Schultz: DNA-based assembly of gold nanocrystals. *Angew Chem. Int. Ed.* **38,** 1808 (1999).
7. S. Park, A.A. Lazarides, C.A. Mirkin, and R.L. Letsinger: Directed assembly of periodic materials from protein and oligonucleotide-modified nanoparticle building blocks. *Angew. Chem. Int. Ed. Engl.* **40,** 2909 (2001).
8. S.R. Whaley, D.S. English, E.L. Hu, P.F. Barbara, and A.M. Belcher: Selection of peptides with semiconductor binding specificity for directed nanocrystal assembly. *Nature* **405,** 665 (2000).
9. R.D. Piner, J. Zhu, F. Xu, S. Hong, and C.A. Mirkin: "Dip-pen" nanolithography. *Science* **283,** 661 (1999).
10. T.R. Hughes, M. Mao, A.R. Jones, J. Burchard, M.J. Marton, K.W. Shannon, S.M. Lefkowitz, M. Ziman, J.M. Schelter, M.R. Meyer, S. Kobayashi, C. Davis, H. Dai, Y.D. He, S.B. Stephaniants, G. Cavet, W.L. Walker, A. West, E. Coffey, D.D. Shoemaker, R. Stoughton, A.P. Blanchard, S.H. Friend, and P.S. Linsley: Expression profiling using microarrays fabricated by an ink-jet oligonucleotide synthesizer. *Nat. Biotechnol.* **19,** 342 (2001).
11. X. Duan, Y. Huang, Y. Cui, J. Wang, and C.M. Lieber: Indium phosphide nanowires as building blocks for nanoscale electronic and optoelectronic devices. *Nature* **409,** 66 (2001).
12. P.A. Smith, C.D. Nordquist, T.N. Jackson, T.S. Mayer, B.R. Martin, J. Mbindyo, and T.E. Mallouk: Electric-field assisted assembly and alignment of metallic nanowires. *Appl. Phys. Lett.* **77,** 1399 (2000).
13. S.V. Kalinin, D.A. Bonnell, T. Alvarez, X. Lei, Z. Hu, and J.H. Ferris: Atomic polarization and local reactivity on ferroelectric surfaces: A new route toward complex nanostructures. *Nano Lett.* **2,** 589 (2002).
14. J.L. Giocondi and G.S. Rohrer: Spatially selective photochemical reduction of silver on the surface of ferroelectric barium titanate. *Chem. Mater.* **13,** 241 (2001).
15. J.L. Giocondi and G.S. Rohrer: Spatial separation of photochemical oxidation and reductions on the surface of ferroelectric $BaTiO_3$. *J. Am. Ceram. Soc.* **86,** 1182 (2003).
16. J.L. Giocondi and G.S. Rohrer: Structure sensitivity of photochemical oxidation and reductions on $SrTiO_3$ surfaces. *J. Phys. Chem. B* **105,** 8275 (2001).
17. J.H. Ferris, D.B. Li, S.V. Kalinin, and D.A. Bonnell: Nanoscale domain patterning of lead zirconate titanate materials using electron beams. *Appl. Phys. Lett.* **84,** 774 (2004).
18. S.V. Kalinin and D.A. Bonnell: Screening phenomena on oxide surfaces and its implications for local electrostatic and transport measurements. *Nano Lett.* **4,** 555 (2004).
19. J. Lu, E. Delamarche, L. Eng, R. Bennewitz, E. Meyer, and H.J. Guntherodt: Kelvin probe force microscopy on surfaces: Investigation of the surface potential of self-assembled monolayers on gold. *Langmuir* **15,** 8184 (1999).
20. H.R. Zeng, Q.R. Yin, G.R. Li, H.S. Luo, and Z.K. Xu: Abnormal piezoresponse behavior of $Pb(Mg_{1/3}Nb_{2/3})O_3$–30%$PbTiO_3$ single crystal studied by high-vacuum scanning force microscope. *J. Cryst. Growth* **254,** 432 (2003).
21. D.A. Bonnell and R. Shao: Local behavior of complex materials: Scanning probes and nanostructure. *Curr. Opin. Solid State Mater. Sci.* **7,** 161 (2003).
22. C. Wang, H. Lin, and C. Tang: Thermal characterization and microstructure change of cobalt oxides. *Catal. Lett.* **94,** 69 (2004).